

Evolution of the optimal trial wave function with interactions in fractional Chern insulators

Yumin Luan,¹ Yinhan Zhang,¹ and Junren Shi^{1,2,*}

¹*International Center for Quantum Materials, Peking University, Beijing 100871, China*

²*Collaborative Innovation Center of Quantum Matter, Beijing 100871, China*

(Dated: September 8, 2021)

We show that the optimal trial wave function of a fractional Chern insulator depends on the form of its electron-electron interaction. The gauge of single particle Bloch bases for constructing the optimal trial wave function is obtained by applying the variational principle proposed by Zhang *et al.* [Phys. Rev. B **93**, 165129 (2016)]. We consider a short-range interaction, the Coulomb interaction, and an interpolation between them, and determine the evolution of the optimal gauge with the different interactions. We compare the optimal gauge with those proposed by Qi [Phys. Rev. Lett. **107**, 126803 (2011)] and Wu *et al.* [Phys. Rev. B **86**, 085129 (2012)], and find that Wu *et al.*'s gauge is close to the optimal gauge when the interaction is a certain mixture of the Coulomb interaction and the short-range interaction, while Qi's gauge is qualitatively different from the optimal gauge in all the cases. Both the gauges deviate significantly from the optimal gauge when the short-range component of the interaction becomes more prominent.

I. INTRODUCTION

Fractional quantum Hall effect (FQHE), which exhibits fractional plateau of the Hall conductance in high magnetic field and low temperature [1], is one of the most important discoveries of condensed matter physics. Different from the single particle nature of the integer quantum Hall effect (IQHE) [2, 3], the FQHE is driven by electron-electron interaction [4–7]. Actually, it is the first topological state ever discovered that is induced by an interaction. For the reason, the study of the effect occupies a center position in theoretical inquiries of condensed matter physics. Moreover, some of FQH states could even find potential applications in topological quantum computing because they support excitations of non-Abelian statistics, which could be utilized to encode quantum information free from local disturbances [8, 9].

Recently, theoretical studies reveal a new class of lattice models that exhibit FQH states without a magnetic field [10–14]. All of these models possess at least a flat Chern band that is nearly dispersionless and isolated from other bands by energy gaps, and is topologically nontrivial with a nonzero Chern number. The band imitates a Landau level in ordinary FQH systems. Similar to the case of a Landau level, in the presence of an electron-electron interaction, the band with a fractional filling factor could also exhibit the FQHE, resulting in a fractional Chern insulator (FCI) [15–18]. The important and remarkable feature of FCIs is that they can potentially be realized in zero magnetic field and high temperature [12, 13], which is highly desirable for applications.

In order to understand the FQH physics arisen in FCIs, it is important to find a way to construct their many-body ground state wave functions, as Laughlin's wave function for ordinary FQH systems [4]. To this end, Qi

proposes a mapping approach which obtains the ground state wave function of a FCI from a FQH wave function of the same filling fraction [19]. Specifically, one expands a FQH many-body wave function in single-body Landau orbitals. By replacing the single-body Landau orbitals with a set of single-body bases constructed in a FCI, we obtain a ground state trial wave function for the FCI. Unfortunately, the mapping method suffers from the arbitrariness of the choices of the Landau orbitals and the FCI bases, as well as the correspondence between them. In this aspect, Qi chooses LLL orbitals in the Landau gauge on a cylinder, and map them to a set of one-dimensional localized Wannier functions constructed in the flat Chern band of a FCI [19]. Wu *et al.* adopt an alternative mapping by considering the effect of finite-size and analogousness of phase between LLL orbitals and Wannier orbitals of a FCI. It achieves a higher overlap with the exact ground state wave function of a FCI compared to Qi's approach [20–22].

Zhang *et al.* indicate that the arbitrariness is actually the choice of a gauge for constructing two-dimensional (2D) localized Wannier functions when mapping a continuous system to a lattice model. From the observation, they establish a general variational principle for determining the optimal gauge that minimizes the interaction energy [23]. An immediate consequence from the consideration is that the optimal gauge should depend on the form of the interaction adopted in a FCI model. This is in sharp contrast with Qi's or Wu *et al.*'s approaches, both of which prescribe a single mapping for all possible FCI models derived from one lattice model but with different forms of interaction. While the general principle is established in Ref. [23], its manifestation in a real FCI model was not explicitly demonstrated. It would be desirable to see how the different forms of interaction affect the optimal gauge, and how Qi's and Wu *et al.*'s choices of the gauge are compared to the optimal one.

In this paper, we demonstrate the dependence of the optimal gauge (or equivalently, the optimal trial ground

* junrenshi@pku.edu.cn

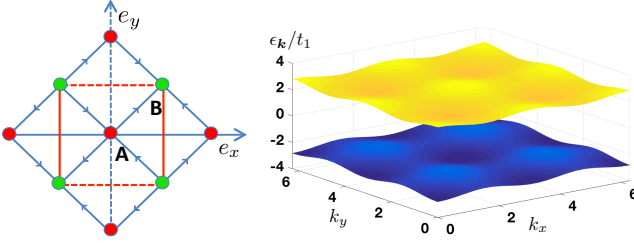


Figure 1. (Color online) Left: Lattice configuration of the checkerboard model. Each unit cell, which is defined as the area enclosed by the red lines, contains two sites A (red circles) and B (green circles). Lattice vectors are $\mathbf{a}_x \equiv (1, 0)$ and $\mathbf{a}_y \equiv (0, 1)$. The NN hopping amplitudes represented by arrows direction is $t_1 \exp(i\pi/4)$, and the NNN hopping amplitudes, represented by dashed lines and solid lines, are $-t_2$ and t_2 , respectively. Right: The flat Chern bands of the checkerboard lattice model with parameters $t_1 = \sqrt{2}t_2$.

state wave function) on different forms of electron-electron interaction in the checkerboard model [10–12, 14]. The optimal gauge is determined by the interaction energy variational principle proposed by Zhang *et al.* [23]. We consider three forms of interaction, including a short-range interaction which is widely adopted in literatures, the Coulomb interaction, and an interpolation between them. We find that, when varying the form of interaction, the optimal gauge changes significantly. The corresponding Wannier functions, which facilitate the mapping from Landau levels in continuous space to the lattice model, also change in both spatial distribution and symmetry. We compare the optimal gauge with those determined by Qi's proposal and Wu *et al.*'s proposal. We find that Wu *et al.*'s gauge can be close to the optimal gauge when the interaction is a certain mixture of the Coulomb interaction and the short-range interaction, while Qi's gauge is qualitatively different from the optimal gauge with a different spatial symmetry for all the cases. Both the gauges deviate the optimal one significantly when the short-range component of the interaction becomes more prominent.

The remainder of the article is organized as follows. In Sec. II, we present the tight-binding model of the checkerboard lattice, and three forms of the interaction surveyed in the present work are introduced. The method for determining the optimal gauge as well as its numerical implementation are discussed. In Sec. III, we present the results of the optimal gauges for the three forms of interaction. Finally, Sec. IV contains a concluding remark.

II. MODEL AND METHODS

A. Lattice model

A large number of flat Chern band models of various lattice configurations had been proposed in literatures. These include models with a checkerboard lattice [10–12,

14], a kagome lattice [13], and a honeycomb lattice [14], all of which possess a flat band with a Chern number $C = \pm 1$. Models with a higher Chern number had also been proposed in such as pyrochlore slabs [24–26], dice lattice [27], and triangle lattice [28–30]. In this paper, for simplicity, we choose the checkerboard lattice model as our system for demonstrating the interaction dependence of the optimal trial wave function of FCIs.

The lattice configuration of the checkerboard model is shown in the left panel of Fig. 1. The tight-binding Hamiltonian of the model with nearest-neighbor (NN) and next-nearest-neighbor (NNN) hopping terms can be expressed, in the reciprocal space, as [12]:

$$H = \sum_{\mathbf{k}} \psi_{\mathbf{k}}^\dagger \mathcal{H}_{\mathbf{k}} \psi_{\mathbf{k}}, \quad \mathcal{H}_{\mathbf{k}} = \mathbf{T}(\mathbf{k}) \cdot \boldsymbol{\sigma},$$

$$T_1(\mathbf{k}) - iT_2(\mathbf{k}) = t_1 e^{-i\frac{\pi}{4}} [1 + e^{i(k_y - k_x)}]$$

$$+ t_1 e^{i\frac{\pi}{4}} [e^{-ik_x} + e^{ik_y}], \quad (1)$$

$$T_3(\mathbf{k}) = 2t_2 (\cos k_x - \cos k_y), \quad (2)$$

where $\psi_{\mathbf{k}} \equiv (\alpha_{\mathbf{k}A}, \alpha_{\mathbf{k}B})^T$ with $\alpha_{\mathbf{k}\tau}$ being the annihilate operator for a state with a wave vector \mathbf{k} and at the sublattice $\tau = A, B$, and $\boldsymbol{\sigma} \equiv (\sigma_1, \sigma_2, \sigma_3)$ with σ_i , $i = 1, 2, 3$ being the Pauli matrices. $T_1(\mathbf{k})$ and $T_2(\mathbf{k})$ correspond to the NN term between A site and B site, while $T_3(\mathbf{k})$ is the NNN hopping term in the same sub-lattice, and t_1 and t_2 are respective hopping constants. When $t_1 = \sqrt{2}t_2$, the bands become flattest [12]. The right panel of Fig. 1 shows the band structure under this condition.

One can diagonalize the Hamiltonian, and obtains two eigenvalues $\epsilon_{1,2}(\mathbf{k}) = \mp |\mathbf{T}(\mathbf{k})|$ as well as eigenvectors $u_{1,2}(\mathbf{k})$:

$$u_1(\mathbf{k}) = \begin{pmatrix} e^{-\frac{i}{2}\gamma_{\mathbf{k}}} \sin \frac{\varphi_{\mathbf{k}}}{2} \\ -e^{\frac{i}{2}\gamma_{\mathbf{k}}} \cos \frac{\varphi_{\mathbf{k}}}{2} \end{pmatrix}, \quad u_2(\mathbf{k}) = \begin{pmatrix} e^{-\frac{i}{2}\gamma_{\mathbf{k}}} \cos \frac{\varphi_{\mathbf{k}}}{2} \\ e^{\frac{i}{2}\gamma_{\mathbf{k}}} \sin \frac{\varphi_{\mathbf{k}}}{2} \end{pmatrix}, \quad (3)$$

where $\tan \gamma_{\mathbf{k}} = T_2(\mathbf{k})/T_1(\mathbf{k})$ and $\cos \varphi_{\mathbf{k}} = T_3(\mathbf{k})/|\mathbf{T}(\mathbf{k})|$. The Chern number of a band can be calculated by integrating the Berry curvature $\Omega_i(\mathbf{k})$, $i = 1, 2$ over the Brillouin zone (BZ) $C_i = (1/2\pi) \int_{\text{BZ}} \Omega_i(\mathbf{k}) dk_x dk_y$, with $\Omega_i(\mathbf{k}) = [\nabla_{\mathbf{k}} \times \mathbf{A}_i(\mathbf{k})]_z$, and $\mathbf{A}_i(\mathbf{k}) = i \langle u_i(\mathbf{k}) | \nabla_{\mathbf{k}} | u_i(\mathbf{k}) \rangle$ is the Berry connection of the band. For the checkerboard lattice model, the Chern number is found to be $C_{1,2} = \pm 1$. With a partially filled topological flat band and in the presence of an electron-electron interaction, the system would become a FCI, as demonstrated in Ref. [12].

B. Interactions

While a flat Chern band provides a playground for electrons, it is the electron-electron interaction that drives the system to a FCI state. The interaction is usually assumed to have the form of the density-density

coupling, which in general can be written as $\hat{h}_{\text{int}} = \sum_{i,j,\tau_1,\tau_2} V^{\tau_1\tau_2}(\mathbf{R}_i - \mathbf{R}_j) \hat{n}_{i\tau_1} \hat{n}_{j\tau_2}$, where $\hat{n}_{i\tau}$ is the particle number operator at the τ sub-lattice of the unit cell i . Since only the partially filled flat band is relevant to the FCI, one can project the interaction to the band and obtain $\hat{h}_{\text{int}}^p = 1/N \sum_{\mathbf{k}_1, \mathbf{k}_2, \mathbf{q}} M(\mathbf{k}_1, \mathbf{k}_2; \mathbf{q}) \hat{\rho}_{\mathbf{k}_1, \mathbf{q}} \hat{\rho}_{\mathbf{k}_2, -\mathbf{q}}$, where $\hat{\rho}_{\mathbf{k}, \mathbf{q}} = \hat{d}_{\mathbf{k}+\mathbf{q}}^\dagger \hat{d}_{\mathbf{k}}$, $\hat{d}_{\mathbf{k}}$ ($\hat{d}_{\mathbf{k}}^\dagger$) is the annihilation (creation) operator for a Bloch state in the topological flat band, and N is the total number of unit cells. The interaction matrix element $M(\mathbf{k}_1, \mathbf{k}_2; \mathbf{q})$ can be written as:

$$M(\mathbf{k}_1, \mathbf{k}_2; \mathbf{q}) = \sum_{\tau_1, \tau_2} V_{\mathbf{q}}^{\tau_1\tau_2} u_{1,\tau_1}^*(\mathbf{k}_1 + \mathbf{q}) \times u_{1,\tau_1}(\mathbf{k}_1) u_{1,\tau_2}^*(\mathbf{k}_2 - \mathbf{q}) u_{1,\tau_2}(\mathbf{k}_2) \quad (4)$$

where $u_{1,\tau}$ is the τ -component of the eigenvector Eq. (3), $V_{\mathbf{q}}^{\tau_1\tau_2} = \sum_{\mathbf{R}} V^{\tau_1\tau_2}(\mathbf{R}) \exp(-i\mathbf{q} \cdot \mathbf{R})$, and we have assumed that the band 1 is partially filled.

In literatures, the interaction is usually assumed to be of a short-range one which only couples between NNs. It has the form:

$$V^{\tau_1\tau_2}(\mathbf{R}_i - \mathbf{R}_j) = \begin{cases} U_1 & i\tau_1, j\tau_2 \in NN \\ 0 & \text{others} \end{cases}, \quad (5)$$

In the checkerboard lattice model, it corresponds to:

$$V_{\mathbf{q}} = \begin{bmatrix} 0 & U_1(\mathbf{q}) \\ U_1^*(\mathbf{q}) & 0 \end{bmatrix}, \quad (6)$$

where $U_1(\mathbf{q}) = U_1(1 + e^{-iq_1} + e^{-iq_2} + e^{-i(q_1+q_2)/2})$.

While the short-range interaction is convenient for numerical simulations, it is nevertheless very different from interactions in real systems. In real materials, the interaction between two electrons that are spatially far apart should be the Coulomb interaction:

$$V^{\tau_1\tau_2}(\mathbf{R}_i - \mathbf{R}_j) = \frac{U_2}{|\mathbf{r}_i^{\tau_1} - \mathbf{r}_j^{\tau_2}|}, \quad (7)$$

where $\mathbf{r}_i^{\tau_1}$ represents the real-space position of the given lattice site. The interacting potential corresponds to:

$$V_{\mathbf{q}} = \begin{bmatrix} U_2(\mathbf{q}) & U_2'(\mathbf{q}) \\ U_2'^*(\mathbf{q}) & U_2(\mathbf{q}) \end{bmatrix}, \quad (8)$$

where $U_2(\mathbf{q}) = 2\pi U_2 \sum_{\mathbf{G}} |\mathbf{q} + \mathbf{G}|^{-1}$, $U_2'(\mathbf{q}) = 2\pi U_2 \exp(-i\mathbf{q} \cdot \boldsymbol{\tau}) \sum_{\mathbf{G}} (-1)^{m+n} |\mathbf{q} + \mathbf{G}|^{-1}$, $\boldsymbol{\tau} = (\frac{1}{2}, \frac{1}{2})$ is a vector from A site to B site, and the summation is over the reciprocal lattice vectors $\mathbf{G} = 2\pi(m, n)$.

Moreover, one expects that the electron-electron interaction should deviate from the Coulomb interaction at short distances. This is because an electron in a lattice site of the tight-binding model is actually corresponded to a finite size electron cloud with a spatial distribution

instead of an ideal point charge. To take account of the deviation, we introduce an interaction which mixes the short-range interaction and the Coulomb interaction. It reads,

$$V^{\tau_1\tau_2}(\mathbf{R}_i - \mathbf{R}_j) = \begin{cases} U_1, & i\tau_1, j\tau_2 \in NN \\ \frac{U_2}{|\mathbf{r}_i^{\tau_1} - \mathbf{r}_j^{\tau_2}|}, & i\tau_1, j\tau_2 \notin NN \end{cases}. \quad (9)$$

The interaction is an interpolation between the short-range interaction and the Coulomb interaction, and the ratio U_2/U_1 controls the relative strengths of the two components. The interaction becomes the pure Coulomb interaction when $U_2/U_1 = 1/\sqrt{2}$, while the short-range component becomes more prominent when U_2/U_1 deviates from the ratio.

The interactions introduced in Eq. (5), Eq. (7) and Eq. (9) are three representative forms which we will survey in this paper. We will determine optimal gauges corresponding to them and demonstrate how the form of interaction affects the construction of the trial ground state wave function.

C. Methods

We determine the optimal gauge by using the variational principle of interaction energy proposed by Zhang *et al.* [23]. The gauge is represented by a function $\theta(\mathbf{k})$, which assigns a $U(1)$ phase to each of the Bloch states in the BZ. The gauge determines the spatial distributions of the 2D localized Wannier functions which facilitate the mapping from Landau levels to a FCI lattice model, and acts as variational parameters for the trial ground state wave function. Accordingly, $\theta(\mathbf{k})$ are determined by the variational principle of ground state energy, which is equivalent to minimizing the interaction energy functional [23]:

$$E_{\text{int}}[\theta(\mathbf{k})] = \frac{1}{N} \sum_{\mathbf{k}_1, \mathbf{k}_2, \mathbf{q}} M(\mathbf{k}_1, \mathbf{k}_2; \mathbf{q}) \Pi(\mathbf{k}_1 - \mathbf{k}_2; \mathbf{q}) \times e^{-i[\theta(\mathbf{k}_1 + \mathbf{q}) - \theta(\mathbf{k}_1) + \theta(\mathbf{k}_2 - \mathbf{q}) - \theta(\mathbf{k}_2)]} \quad (10)$$

where $\Pi(\mathbf{k}_1 - \mathbf{k}_2; \mathbf{q})$ is the two-particle correlation function of the FQH state to be mapped, and can be determined by [23]:

$$\Pi(\mathbf{k}_1 - \mathbf{k}_2; \mathbf{q}) = \nu^2 (\delta_{\mathbf{q},0} - \delta_{\mathbf{k}_1 - \mathbf{k}_2 + \mathbf{q},0}) + e^{-i(\mathbf{A}_{\mathbf{k}_1 + \mathbf{q}}^L - \mathbf{A}_{\mathbf{k}_2}^L) \cdot \mathbf{q}} \Pi'(\mathbf{k}_1 - \mathbf{k}_2; \mathbf{q}), \quad (11)$$

$$\Pi'(\mathbf{k}; \mathbf{q}) = \frac{1}{N} \sum_{\mathbf{R}} \Pi'(\mathbf{R}; \mathbf{q}) e^{-i\mathbf{k} \cdot \mathbf{R}}, \quad (12)$$

$$\begin{aligned} \Pi'(\mathbf{R}; \mathbf{q}) = & 2\nu^2 \exp \left[-i\mathbf{q} \cdot \mathbf{R} - \frac{1}{2l_M^2} (\mathbf{R} - \hat{z} \times \mathbf{q} C_1 l_M^2)^2 \right] \\ & \times \sum_{k=0}^{\infty} c_{2k+1} L_{2k+1} \left(\frac{1}{l_M^2} (\mathbf{R} - \hat{z} \times \mathbf{q} C_1 l_M^2)^2 \right) \end{aligned} \quad (13)$$

where ν is the filling factor, \mathbf{R} denotes a lattice vector, $\mathbf{A}_{\mathbf{k}}^L = (-C_1 k_2 / 2\pi, 0)$, $l_M = 1/\sqrt{2\pi}$, $L_n(x)$ is the Laguerre function, and the coefficients c_{2k+1} for $\nu = 1/3$ and $1/5$ can be found in Ref. [31].

We define the correlation energy $E_{\text{corr}} = E_{\text{int}} - E_{\text{HF}}$, where E_{HF} is the mean-field interacting energy determined by the Hartree-Fock approximation, and can be written as:

$$E_{\text{HF}} = \frac{1}{N} \sum_{\mathbf{k}_1, \mathbf{k}_2} M(\mathbf{k}_1, \mathbf{k}_2; 0) \nu - M(\mathbf{k}_1, \mathbf{k}_2; \mathbf{k}_2 - \mathbf{k}_1) \nu (1 - \nu), \quad (14)$$

which is independent of the choice of the gauge. Different choices of the gauge affect how electrons are correlated locally, and give rise to different correlation energies. We adopt the correlation energy as an indicator for the quality of a trial ground state wave function.

The function $\theta(\mathbf{k})$ can be used to construct the projected Wannier functions [23]:

$$w_{\tau}(\mathbf{r}, \mathbf{R}) = \frac{1}{\sqrt{N}} \sum_{\mathbf{k}} \varphi_{1\mathbf{k}}(\mathbf{r}) u_{1,\tau}^*(\mathbf{k}) \exp(-i\mathbf{k} \cdot \mathbf{R} - i\theta(\mathbf{k})) \quad (15)$$

where $\varphi_{1\mathbf{k}}(\mathbf{r})$ is a magnetic Bloch wave function of the LLL with the same Chern number C_1 as the partially filled flat Chern band. The gauge of $\varphi_{1\mathbf{k}}(\mathbf{r})$ and $u_1(\mathbf{k})$ should be regularized to satisfy the same quasi-periodic conditions for $\psi_{\mathbf{k}} \equiv \varphi_{1\mathbf{k}}$ or $u_1(\mathbf{k})$:

$$\begin{aligned} \psi_{\mathbf{k}+\mathbf{K}_1} &= \psi_{\mathbf{k}}, \\ \psi_{\mathbf{k}+\mathbf{K}_2} &= \psi_{\mathbf{k}} \exp(iC_1 k_1), \end{aligned} \quad (16)$$

where $\mathbf{K}_1 = 2\pi(1, 0)$, $\mathbf{K}_2 = 2\pi(0, 1)$. The Wannier functions are spatially localized and can be employed to map a Landau level to the partially filled flat Chern band.

The mapping facilitated by the Wannier functions is equivalent to mapping the magnetic Bloch wave functions $\varphi_{1\mathbf{k}}$ to the lattice Bloch wave functions $u_1(\mathbf{k}) e^{i\theta(\mathbf{k})}$, through which $\{\theta(\mathbf{k})\}$ become variational parameters of the trial ground state wave function. While mappings with different $\{\theta(\mathbf{k})\}$ lead to the same kinetic part of a FCI hamiltonian, their interaction energies will be different due to different density distributions of the Wannier functions. A direct application of the variational principle of ground state energy immediately leads to the variational principle dictated by the interaction energy functional Eq. (10).

D. Numerical implementation

We implement our numerical calculation in a discretized BZ with a 21×21 mesh of \mathbf{k} points. In the real space, it corresponds to a finite size lattice with 21×21 unit cells and periodic boundary conditions. The size is much larger than the coherence length beyond which $\Pi'(\mathbf{R}, \mathbf{q})$ approaches a constant (See Fig. 3 of Ref. [23]). We focus on the case of a $\nu = 1/3$ filled band which is a counterpart of the FQH state with the filling factor $\nu = 1/3$.

The regularized Bloch wave functions consistent with the quasi-periodic conditions Eq. (16) can be explicitly chosen. For the magnetic Bloch wave functions, we adopt the form:

$$\begin{aligned} \varphi_{1\mathbf{k}}(\mathbf{r}) = & \left(\frac{\sqrt{2}}{N} \right)^{\frac{1}{2}} \sum_{m \in \mathbb{Z}} \exp[-iC_1 k_1 m + i(k_2 + 2\pi m)y] \\ & \times \exp \left[-\pi \left(x + k_2 / 2\pi + m \right)^2 \right]. \end{aligned} \quad (17)$$

The lattice Bloch wave function $u_1(\mathbf{k})$ can be regularized in the discretized BZ. Starting from $u_1(\mathbf{k} = 0)$, the phases for the wave functions along the k_2 axis are chosen to satisfy the condition:

$$\text{Im}[\langle u_{0,n} | u_{0,n+1} \rangle] = 0, \text{Re}[\langle u_{0,n} | u_{0,n+1} \rangle] > 0, \quad (18)$$

for $n = 0 \dots M-2$, where $u_{m,n}$ denotes the lattice Bloch wave function $u_1(\mathbf{k})$ at the mesh point (m, n) of the discretized BZ, and $M = 21$ is the size of the mesh. Then, the phases of other Bloch wave functions are chosen to satisfy the condition:

$$\text{Im}[\langle u_{m,n} | u_{m+1,n} \rangle] = 0, \text{Re}[\langle u_{m,n} | u_{m+1,n} \rangle] > 0, \quad (19)$$

for $m = 0 \dots M-2$, $n = 0 \dots M-1$. Finally, we make a global gauge transformation:

$$u_{m,n} \rightarrow u_{m,n} \exp \left[-\frac{i}{M} (n\delta_0 + m\delta_n) \right], \quad (20)$$

where $\delta_0 = \arg\langle u_{0,0} | u_{0,M-1} \rangle$, and $\delta_n = \langle u_{0,n} | u_{M-1,n} \rangle$. These regularized wave functions define our initial gauge, which corresponds to $\theta(\mathbf{k}) = 0$ in the energy functional Eq. (10). It turns out that the initial gauge is exactly the gauge adopted in Qi's approach [19, 23].

To determine $\theta(\mathbf{k})$ that minimizes the energy functional, we employ the steepest descent algorithm. We run multiple iterations starting from different initial values, and check whether they converge to the same result. In this way, convergences to global minimums are guaranteed.

III. RESULTS

A. Optimal gauge for the short-range interaction

We determine the optimal gauge for the short-range interaction defined in Eq. (5). The distribution of $\theta(\mathbf{k})$

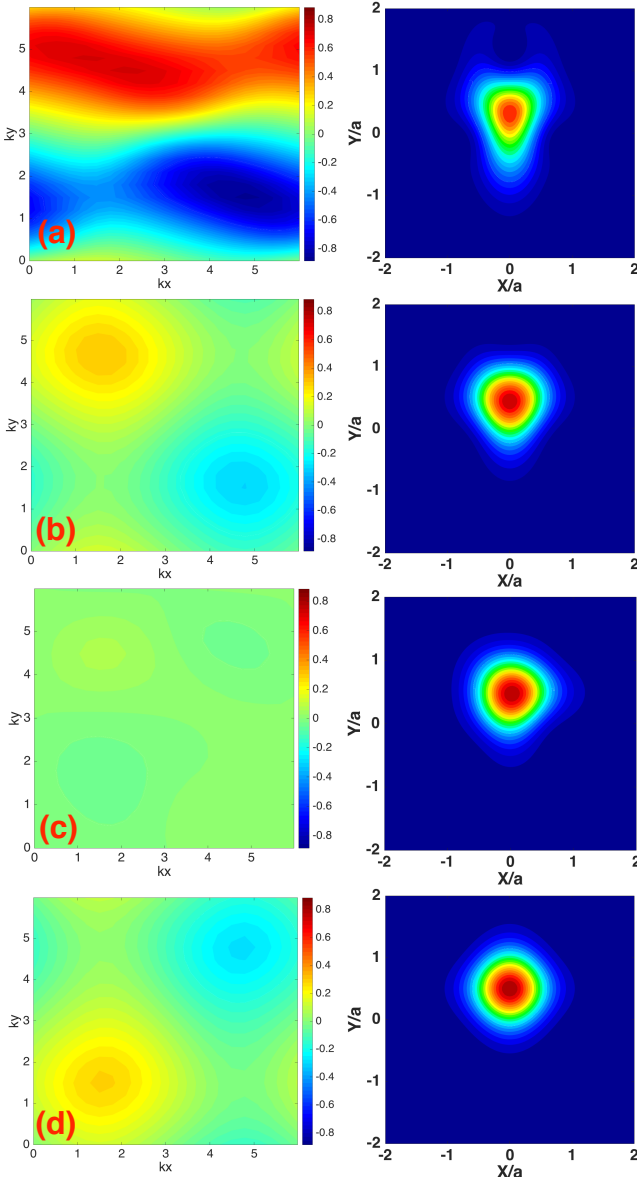


Figure 2. (Color online) Distributions of $\theta(\mathbf{k})$ (left) in the BZ and the spatial distributions of the corresponding projected Wannier functions at A-site (right) for different gauges. (a) The optimal gauge for the short-range interaction defined in Eq. (5); (b) Wu *et al.*'s gauge; (c) The maximally localized gauge; (d) The symmetric gauge. Qi's gauge corresponds to $\theta(\mathbf{k}) = 0$, and is very close to the maximally localized gauge.

in the BZ and the spatial distribution of corresponding projected Wannier functions at the A-site are shown in the left panel and right panel of Fig. 2(a), respectively. For comparison, we also show results for Wu *et al.*'s gauge [20], the maximally localized gauge that gives rise to a projected Wannier function maximally localized in the real space, as well as a symmetric gauge which gives rise to a C_4 symmetric Wannier function. The last two gauges are defined in Ref. [23]. We find that $\theta(\mathbf{k})$ of the optimal gauge has an amplitude $\sim \pi/4$. It shows a sig-

Table I. Comparison of the interaction energy and the correlation energy per electron for different gauges. Both results for the short-range interaction and the Coulomb interaction are shown. The unit of the energy is U_1 (U_2) for the short-range (Coulomb) interaction.

gauge	Short-range interaction			Coulomb interaction		
	E_{int}	E_{corr}	$\frac{\Delta E_{\text{corr}}}{E_{\text{corr}}^{\text{OP}}}$	E_{int}	E_{corr}	$\frac{\Delta E_{\text{corr}}}{E_{\text{corr}}^{\text{OP}}}$
Qi	0.2893	0.0697	17.74%	11.7061	0.1660	2.72%
Wu <i>et al.</i>	0.2851	0.0655	10.64%	11.7032	0.1631	0.93%
symmetric	0.2921	0.0725	22.47%	11.7079	0.1678	3.84%
Optimal	0.2788	0.0592	/	11.7018	0.1616	/

nificant deviation from the original gauge proposed by Qi, *i.e.* $\theta(\mathbf{k}) = 0$. In comparison, $\theta(\mathbf{k})$ of Wu *et al.*'s gauge has a smaller amplitude $\sim \pi/10$, with a distribution in the BZ qualitatively similar to that of the optimal gauge, *i.e.*, both of them have a peak and a valley located in the same regions of the BZ. It indicates that Wu *et al.*'s gauge, while not optimal, is nevertheless better than Qi's gauge. On the other hand, the maximally localized gauge yields $\theta(\mathbf{k})$ with an amplitude 10^{-2} . It is not identical but very close to Qi's gauge. Reference [23] proves that the maximally localized gauge is the optimal gauge for a soft and isotropic interaction. Hence, Qi's gauge should be good for the case, but is not a good choice for the short-range interaction. Finally, the symmetric gauge has a distribution of $\theta(\mathbf{k})$ distinct from the optimal gauge.

We also show the spatial distributions of the corresponding Wannier functions at the A-site for different gauges in the right panel of Fig. 2. The Wannier function of the B-site can be obtained by a reflection with respect to the diagonal $y = x$. We observe that both the Wannier functions for the optimal gauge and Wu *et al.*'s gauge have the mirror symmetry with respect to the y -axis, while the one for Qi's gauge (or the maximally localized gauge) has the mirror symmetry with respect to the diagonal $y = -x$. It indicates that Qi's gauge is qualitatively different from the optimal one. Comparing Wu *et al.*'s gauge and the optimal gauge, we find that the former is more localized spatially, and the latter is elongated along the y -direction.

Table I shows the comparison of the interaction energies and correlation energies for different gauges in the short-range interaction. Compared to the optimal gauge, the other three gauges show significantly higher ($> 10\%$) correlation energies. Among them, Wu *et al.*'s gauge is closest to the optimal one. The symmetric gauge turns out to be the worst since it is based on an *ad hoc* requirement that the Wannier function should have the same point group symmetry as its hosting lattice.

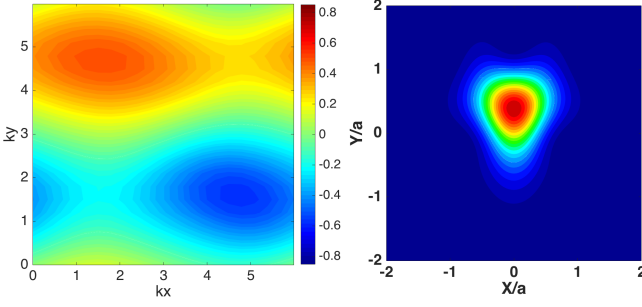


Figure 3. (Color online) Distribution of $\theta(\mathbf{k})$ in the BZ (left) and the spatial distribution of the Wannier function at the A-site (right) of the optimal gauge for the Coulomb interaction.

B. The optimal gauge for the Coulomb interaction

We also determine the optimal gauge for the Coulomb interaction, shown in Fig. 3. Compared to the optimal gauge for the short-range interaction, the Wannier function becomes more localized spatially and shorten along the y direction. The observation is a clear indication that the optimal gauge depends on the form of interaction.

In Table I, we also show that the interaction energy and correlation energy per electron for the Coulomb interaction. We observe that the difference in the energy between different gauges becomes much smaller. This is not surprising because different gauges only change the density distribution of the Wannier function. The local change can only affects the short-range correlations of electrons, and has a relatively minor effect when the interaction is of a long-range one.

C. Evolution of the optimal gauge with interactions

After establishing the dependence of the optimal gauge on the form of interaction, we proceed to see how the optimal gauge evolves with different forms of interactions. We adopt the mixed form of the interaction Eq. (9), and determine optimal gauges for different values of U_2/U_1 . Figure 4 shows the evolution of corresponding Wannier functions. We observe that the overall shapes of the Wannier functions undergo clearly visible changes, from a elongated triangle pointing downward for the short-range interaction ($U_2/U_1 = 0$), to a nearly equilateral triangle pointing downward when $U_2/U_1 = 1$, and to triangles pointing upward when U_2/U_1 is further increased. Actually, the Wannier function for the interaction ($U_2/U_1 \sim 1$) is very close to that in Wu *et al.*'s gauge shown in Fig. 2(b).

In Fig. 5, we show the correlation energy corresponding to Qi's gauge and Wu *et al.*'s gauge relative to that of the optimal gauge versus the ratio U_2/U_1 . We see that the correlation energies of both the gauges can be close to that of the optimal gauge when the strengths of the short-range interaction and the Coulomb interaction

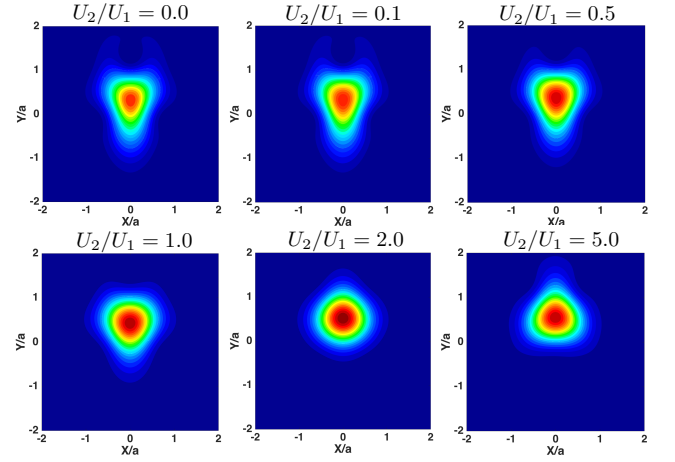


Figure 4. (Color online) Evolution of the Wannier function of the optimal gauge for the mixed form of interaction Eq. (9) with the ratio U_2/U_1 varied from 0.0 to 5.0. $U_2/U_1 = 0$ corresponds to the short-range interaction Eq. (5), and $U_2/U_1 = 1.0$ corresponds to the case where the Wannier function is very close to that in Wu *et al.*'s gauge.

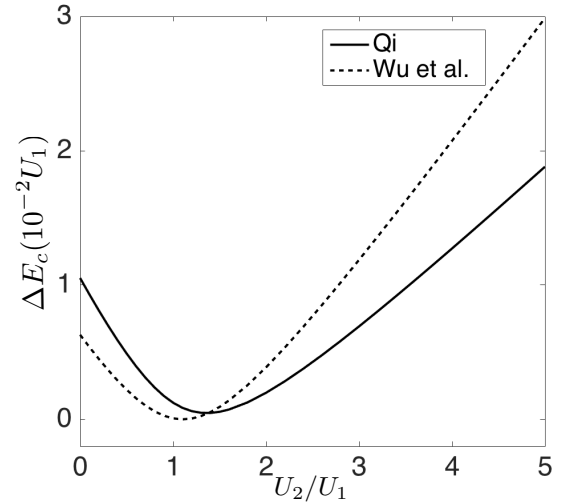


Figure 5. Correlation energies versus U_2/U_1 of Qi's gauge and Wu *et al.*'s gauge relative to the optimal one.

are approximately equal ($U_2/U_1 \sim 1$), but deviate significantly when the short-range component of the interaction becomes more prominent ($U_2/U_1 \ll 1$ or $\gg 1$). This is not surprising because our variational degrees of freedom $\theta(\mathbf{k})$ affects mainly short-range correlations in the trial ground state wave function by modifying the spatial distribution of the Wannier functions. Its effect to a system with a long-range interaction like the Coulomb interaction would be minimal. We also observe that while Wu *et al.*'s gauge can be very close to the optimal gauge when $U_2/U_1 \approx 1$, it actually becomes worse than Qi's gauge when $U_2/U_1 \gg 1$. This is because in the regime, both the gauges are qualitatively different from the optimal

gauge, and Qi's gauge is actually relatively closer to the optimal one, as evident from Fig. 4 and Fig. 2(b, c).

IV. CONCLUDING REMARK

In conclusion, we have demonstrated the evolution of the optimal gauge for constructing the trial wave function of the FCI in the checkerboard model. It clearly

indicates that the optimal gauge is not only determined by the kinetic property of a flat Chern band, but also the form of interaction. We also compare the optimal gauge with those proposed by Qi and Wu *et al.*. We find that both the gauges deviate from the optimal one when the short-range component in the interaction becomes more prominent, although Wu *et al.*'s gauge can be very close to the optimal gauge for a certain mixture of the short-range interaction and the Coulomb interaction ($U_2/U_1 \sim 1$).

-
- [1] D. C. Tsui, H. L. Stormer and A. C. Gossard, Phys. Rev. Lett. **48**, 1559 (1982).
 - [2] K. v. Klitzing, G. Dorda and M. Pepper, Phys. Rev. Lett. **45**, 494 (1980).
 - [3] D. J. Thouless, M. Kohmoto, M. P. Nightingale and M. den Nijs, **49**, 405 (1982).
 - [4] R. B. Laughlin, Phys. Rev. Lett. **50**, 1395 (1983).
 - [5] J. K. Jain, Phys. Rev. Lett. **63**, 199 (1989).
 - [6] J. K. Jain, *Composite Fermions* (Cambridge University Press, Cambridge, England, 2007).
 - [7] F. D. M. Haldane, Phys. Rev. Lett. **51**, 605 (1983).
 - [8] G. Moore and N. Read, Nucl. Phys. B **360**, 362(1991) See also N. Read and G. Moore, Prog. Theor. Phys. Suppl. **107**, 157 (1992).
 - [9] C. Nayak, S. H. Simon, A. Stern, M. Freedman and S. Das Sarma, Rev. Mod. Phys. **80**, 1083 (2008).
 - [10] D. N. Sheng, Z. Gu, K. Sun, and L. Sheng, Nature Commun. **2**, 389 (2011).
 - [11] K. Sun, Z. Gu, H. Katsura, and S. Das Sarma, Phys. Rev. Lett. **106**, 236803 (2011).
 - [12] T. Neupert, L. Santos, C. Chamon, and C. Mudry, Phys. Rev. Lett. **106**, 236804 (2011).
 - [13] E. Tang, J.-W. Mei, and X.-G. Wen, Phys. Rev. Lett. **106**, 236802 (2011).
 - [14] Y.-F. Wang, Z.-C. Gu, C.-D. Gong, and D. N. Sheng, Phys. Rev. Lett. **107**, 146803 (2011).
 - [15] N. Regnault and B. A. Bernevig, Phys. Rev. X **1**, 021014 (2011).
 - [16] S. A. Parameswaran, R. Roy and S. L. Sondhi, C. R. Physique **14**, 816 (2013).
 - [17] E. J. Bergholtz and Z. Liu, Int. J. Mod. Phys. B **27**, 1330017 (2013).
 - [18] T. Neupert, C. Chamon, T. Iadecola, L. H. Santos and C. Mudry, Phys. Scr. T164 (2015) 014005 (9pp).
 - [19] X. L. Qi, Phys. Rev. Lett, **107**, 126803 (2011).
 - [20] Y. L. Wu, N. Regnault and B. A. Bernevig, Phys. Rev. B **86**, 085129 (2012).
 - [21] Y. L. Wu, N. Regnault and B. A. Bernevig, Phys. Rev. Lett. **110**, 106802 (2013).
 - [22] Y. L. Wu, N. Regnault and B. A. Bernevig, Phys. Rev. B **89**, 155113 (2014).
 - [23] Y. H. Zhang and J. R. Shi, Phys. Rev. B **93**, 165129 (2016).
 - [24] Z. Liu, E. J. Bergholtz, H. Fan, and A. M. Lauchli, Phys. Rev. Lett. **109**, 186805 (2012).
 - [25] A. Sterdyniak, C. Repellin, B. Andrei Bernevig, and N. Regnault, Phys. Rev. B **87**, 205137 (2013).
 - [26] M. Trescher and E. J. Bergholtz, Phys. Rev. B **86**, 241111 (2012).
 - [27] F. Wang and Y. Ran, Phys. Rev. B **84**, 241103 (R) (2011).
 - [28] Y.-F. Wang, H. Yao, C.-D. Gong, and D. N. Sheng, Phys. Rev. B **86**, 201101 (2012).
 - [29] S. Yang, Z. C. Gu, K. Sun and S. Das Sarma, Phys. Rev. B **86**, 241112 (2012).
 - [30] N. R. Cooper and R. Moessner, Phys. Rev. Lett. **109**, 215302 (2012).
 - [31] S. M. Girvin, A. H. MacDonald, P. M. Platzman, Phys. Rev. B **33**, 2481 (1986).